

Research Article

Theme: Nanoparticles in Vaccine Delivery
Guest Editor: Aliasger Salem

Safety and Biocompatibility of Carbohydrate-Functionalized Polyanhydride Nanoparticles

Julia E. Vela-Ramirez,¹ Jonathan T. Goodman,¹ Paola M. Boggiatto,² Rajarshi Roychoudhury,³
Nicola L. B. Pohl,³ Jesse M. Hostetter,⁴ Michael J. Wannemuehler,² and Balaji Narasimhan^{1,5}

Received 2 September 2014; accepted 7 November 2014; published online 25 November 2014

ABSTRACT. Carbohydrate functionalization of nanoparticles allows for targeting of C-type lectin receptors. This family of pattern recognition receptors expressed on innate immune cells, such as macrophages and dendritic cells, can be used to modulate immune responses. In this work, the *in vivo* safety profile of carbohydrate-functionalized polyanhydride nanoparticles was analyzed following parenteral and intranasal administration in mice. Polyanhydride nanoparticles based on 1,6-bis-(*p*-carboxyphenoxy)hexane and 1,8-bis-(*p*-carboxyphenoxy)-3,6-dioxaoctane were used. Nanoparticle functionalization with di-mannose (specifically carboxymethyl- α -D-mannopyranosyl-(1,2)-D-mannopyranoside), galactose (specifically carboxymethyl- β -galactoside), or glycolic acid induced no adverse effects after administration based on histopathological evaluation of liver, kidneys, and lungs. Regardless of the polymer formulation, there was no evidence of hepatic or renal damage or dysfunction observed in serum or urine samples. The histological profile of cellular infiltration and the cellular distribution and kinetics in the lungs of mice administered with nanoparticle treatments followed similar behavior as that observed in the lungs of animals administered with saline. Cytokine and chemokine profiles in bronchoalveolar lavage fluid indicated surface chemistry dependence on modest secretion of IL-6, IP-10, and MCP-1; however, there was no evidence of any deleterious histopathological changes. Based on these analyses, carbohydrate-functionalized nanoparticles are safe for *in vivo* applications. These results provide foundational information towards the evaluation of the capabilities of these surface-modified nanoparticles as vaccine delivery formulations.

KEY WORDS: biocompatibility; carbohydrate; nanoparticles; polyanhydride; safety.

INTRODUCTION

The development of novel strategies to improve adjuvant formulations by directly targeting innate immune cells is an important area of interest in the design of novel vaccines (1–4). Biodegradable nanoparticles possess promising characteristics in this regard by playing dual roles, both as adjuvants and delivery vehicles (5). In particular, polyanhydride particles have been demonstrated to induce enhanced expression of MHCs I and II on and stimulation of antigen-presenting cells (APCs), which are fundamental to initiating adaptive immune responses (6–8). After *in vivo* administration, the

nanoparticles interact with a variety of cells, including APCs (9,10). Before analyzing the effects of surface modification upon vaccine efficacy, an assessment of their safety and biocompatibility is necessary (11).

The use of polymeric nanoparticle systems for drug and vaccine delivery offers several advantages, including controlled delivery of encapsulated payload(s) and, depending on their chemical properties, improved biocompatibility, receptor targeting capabilities, sustained antigen/drug release kinetics, adjuvanticity, and opportunities for both local and systemic delivery (12,13). Polyanhydride nanoparticles have displayed these characteristics in both *in vitro* and/or *in vivo* settings (6,9,14–20). In particular, the use of biodegradable nanoparticles for lung delivery is an attractive proposition because of the following advantages: (1) uniform particle distribution in the lung, (2) local administration of vaccine antigens or therapeutic drugs, (3) sustained delivery of macromolecules, (4) improved patient compliance associated with noninvasive immunization and administration of fewer doses, and (5) avoidance of first-pass metabolism, among others (2,12,21–23).

In previous *in vitro* studies, it was demonstrated that di-mannose functionalization of polyanhydride nanoparticles,

¹ Department of Chemical and Biological Engineering, Iowa State University, 2035 Sweeney Hall, Ames, Iowa 50011, USA.

² Department of Veterinary Microbiology and Preventive Medicine, Iowa State University, Ames, Iowa 50011, USA.

³ Department of Chemistry, Indiana University, Bloomington, Indiana 47405, USA.

⁴ Department of Veterinary Pathology, Iowa State University, Ames, Iowa 50011, USA.

⁵ To whom correspondence should be addressed. (e-mail: nbalaji@iastate.edu; nbalaji@iastate.edu)

which would induce signaling *via* C-type lectin receptors (CLRs) on APCs, enhanced the activation of macrophages and dendritic cells (DCs) (6,17,18,24). Because of the role of CLR signaling in stimulating innate immunity, identifying safe and effective means to selectively target APC receptors such as the macrophage mannose receptor (MMR) and the macrophage galactose binding lectin (MGL) will provide novel approaches to enhance and shape adaptive immunity (3,25,26). Both the charge and surface properties of these polyanhydride nanoparticles are altered upon functionalization and could engage additional signaling cascade(s), which may affect the magnitude of immune response to the presence of these functionalized adjuvants/delivery vehicles. In this regard, even though these functionalized particles have displayed desirable properties (*i.e.*, activation of APCs) *in vitro*, the focus of this study was to perform a systematic evaluation of their safety and biocompatibility profile *in vivo* to assess any toxicological effects that might be associated with functionalization.

MATERIALS AND METHODS

Materials

Chemicals needed for monomer synthesis, polymerization, and nanoparticle synthesis included anhydrous (99+%) 1-methyl-2-pyrrolidinone (Aldrich, Milwaukee, WI); 1,6-dibromohexane, 4-*p*-hydroxybenzoic acid, *N,N*-dimethylacetamide, and triethylene glycol (Sigma-Aldrich, St. Louis, MO); 4-*p*-fluorobenzonitrile (Apollo Scientific, Cheshire, UK); and acetic acid, acetic anhydride, acetone, acetonitrile, dimethyl formamide (DMF), hexanes, methylene chloride, pentane, potassium carbonate, sodium hydroxide, sulfuric acid, and toluene (Fisher Scientific, Fairlawn, NJ). For NMR characterization, deuterated dimethyl sulfoxide was purchased from Cambridge Isotope Laboratories (Andover, MA). For nanoparticle tracking Alexa Fluor® 647 hydrazide was purchased from Life Technologies (Grand Island, NY). For nanoparticle functionalization, 1-ethyl-3-(3-dimethylaminopropyl) carbodiimide hydrochloride, *N*-hydroxysuccinimide, and ethylenediamine were purchased from Thermo Scientific (Waltham, MA). Glycolic acid was purchased from Acros Organics (Pittsburgh, PA). Materials required for the lung tissue processing included Dulbecco's Modified Eagle Medium and Hank's balanced salt solution (Life Technologies, Grand Island, NY); HEPES buffer, penicillin-streptomycin, and L-glutamine (Mediatech, Herndon, VA); heat-inactivated fetal bovine serum (Atlanta Biologicals, Atlanta, GA); and ammonium chloride, potassium bicarbonate, 0.5 M EDTA, and sodium azide (Fisher Scientific). β -Mercaptoethanol and rat immunoglobulin (rat IgG) were purchased from Sigma-Aldrich (St. Louis, MO). Materials used for flow cytometry included stabilizing cellular fixative solution (BD Biosciences, San Jose, CA); unlabeled anti-CD16/32 (*i.e.*, anti-Fc γ R) (Southern Biotech, Birmingham, AL); and FITC-conjugated anti-mouse CD11c (clone N418), PE-conjugated anti-mouse CD11b (clone M1/70), Alexa Fluor® 700-conjugated anti-mouse F4/80 (clone BM8), PerCP/Cy5.5-conjugated anti-mouse Ly-6G/Ly-6C (Gr-1) (clone RB6-8C5), PE/Cy7 anti-mouse CD326 (clone G8.8) and their corresponding isotype controls: FITC-

conjugated Armenian Hamster IgG (clone HTK888), PE-conjugated rat IgG2b κ (clone RTK4530), Alexa Fluor® 700-conjugated rat IgG2a κ (clone RTK2758) and PerCP/Cy5.5-conjugated rat IgG2b κ (clone RTK4530), and PE/Cy7-conjugated rat IgG2a κ (clone RTK2758) (BioLegend, San Diego, CA). Endotoxin-free saline was obtained from the Iowa State University College of Veterinary Medicine Pharmacy.

Monomer and Polymer Synthesis

Monomers of 1,6-bis(*p*-carboxyphenoxy)hexane (CPH) and 1,8-bis(*p*-carboxyphenoxy)-3,6-dioxaoctane (CPTEG) were synthesized as described previously (15,27). The 50:50 CPTEG:CPH copolymer was synthesized by melt polycondensation as previously described (15). The chemical structure was characterized with ¹H NMR using a 300-MHz Varian VXR spectrometer (Varian, Inc., Palo Alto, CA). The synthesized 50:50 CPTEG:CPH copolymer had a M_w of 10,500 Da, and the polydispersity index (PDI) of this copolymer was 1.5, which is consistent with previous work (15,20).

Nanoparticle Synthesis

Polyanhydride nanoparticles were synthesized using anti-solvent nanoencapsulation as described previously (28). Briefly, for flow cytometry, Alexa Fluor® 647 hydrazide (1% *w/w*) and 20 mg/mL 50:50 CPTEG:CPH polymer were dissolved in methylene chloride (at 4°C). For histological and cytokine analyses, blank nanoparticles were synthesized. The polymer solution was sonicated at 40 Hz for 30 s using a probe sonicator (Ultra Sonic Processor VC 130PB, Sonics Vibra-Cell, Newtown, CT) and rapidly poured into a pentane bath (at -40°C) at a solvent-to-nonsolvent ratio of 1:250. Particles were collected by filtration and dried under vacuum for 30 min.

Sugar Synthesis

Synthesis of Carboxymethyl α -1,2-Linked Dimannoside

Synthesis of carboxymethyl α -1,2-linked di-mannose was carried out using fluororous solid-phase extraction (FSPE) as per literature procedure (29–31). Each glycosylation was performed with 2.0 equivalents of the donor in anhydrous dichloromethane at 0°C for 15 min. Facile purification of crude product by FSPE enabled easy preparation of the protected linear α -1,2-linked di-mannose in high yield. FSPE was very helpful in the context of this particular synthesis as isolation of the target compound using regular silica gel chromatography turned out to be difficult owing to the formation of unwanted side products (hydrolyzed and rearranged donor). The reducing terminal of the disaccharide was further functionalized by ozonolysis followed by Jones' oxidation to yield a carboxylic acid. Global deprotection was carried out using the Birch reduction condition to produce the desired deprotected dimannoside (6).

Synthesis of Carboxymethyl- β -Galactoside

Allylated β -galactose acetate was subjected to ruthenium-catalyzed sharpless oxidation, which resulted in carboxylic acid-terminated β -galactose acetate in high yield. Base catalyzed deacetylation yielded the desired galactoside in high yield.

Surface Functionalization

Carboxymethyl- α -D-mannopyranosyl-(1,2)-D-mannopyranoside and carboxymethyl- β -galactoside were conjugated onto the surface of polyanhydride nanoparticles using an amine-carboxylic acid coupling reaction (6,17,18,24). Particles with glycolic acid groups on the surface (linker) and non-functionalized (NF) particles were used as controls. The conjugation reaction was performed in two reaction steps, as described previously (6,18). Briefly, a nanoparticle suspension (10 mg/mL) was made using nanopure water, and 10 equivalents of 1-ethyl-3-(3-dimethylaminopropyl)-carbodiimide hydrochloride (EDC) and 12 equivalents of *N*-hydroxysuccinimide (NHS), and 10 equivalents of ethylenediamine were added. This reaction was carried out at a temperature of 4°C for 1 h at a constant agitation of 17 relative centrifugal force (rcf). Following the reaction, the particles were centrifuged at 10,000 rcf for 10 min and the supernatant was removed. The particles were washed with the same volume of nanopure water and centrifuged at 10,000 rcf for 10 min, and the supernatant was removed. A second reaction was performed with 10 equivalents of EDC, 12 equivalents of NHS, and 10 equivalents of the corresponding functionalizing agent (*i.e.*, di-mannose or galactose) in nanopure water, using constant agitation at 17 rcf for 1 h at 4°C. Particles were sonicated before and after each reaction to break aggregates. After the reactions were completed, nanoparticles were collected by centrifugation (10,000 rcf, 10 min) and dried under vacuum for 1 h.

Nanoparticle Characterization

Morphological and size characterization of both the functionalized and the NF nanoparticles was performed using scanning electron microscopy (SEM, FEI Quanta 250, Kyoto, Japan) and quasi-elastic light scattering (QELS, Zetasizer Nano, Malvern Instruments Ltd., Worcester, UK). The QELS experiments were used to measure the ζ -potential of the nanoparticles. To quantify the amounts of the carbohydrates conjugated to the nanoparticles, a high-throughput version of a phenol-sulfuric acid assay was used (6,32). A microplate reader (SpectraMax M3, Molecular Devices, Sunnyvale, CA) was used to obtain the absorbance of standards and samples using a wavelength of 490 nm. The total amount of sugar per unit weight of nanoparticles (micrograms per milligrams) was calculated.

Mice

Female Swiss Webster outbred mice were purchased from Harlan Laboratories (Indianapolis, IN). Mice were housed in specific pathogen-free conditions where all bedding, caging, and feed were sterilized prior to use. All animal

procedures were conducted with the approval of the Iowa State University Institutional Animal Care and Use Committee.

Mouse Treatments

Liver and Kidney Histological and Biomarker Examination

Separate groups of five Swiss Webster outbred mice were subcutaneously injected with 5 mg of polyanhydride nanoparticles (non- or surface-functionalized) in 1.5 mL of phosphate-buffered saline (PBS) at the nape of the neck (33). Control animals received treatment that included alum (100 μ L) or saline (1.5 mL). Urine samples were collected at 7 and 30 days post-administration, prior to necropsy. Whole blood was collected *via* cardiac puncture in heparinated tubes, and liver and kidney tissues were harvested during necropsy and placed in phosphate-buffered formalin. Formalin-fixed tissues at 7 and 30 days post-administration were embedded, sectioned, and stained with hematoxylin and eosin (H&E) and blindly evaluated by a board-certified veterinary pathologist. Histopathological damage caused by inflammation, distribution of inflammatory cells, and tissue necrosis were evaluated using a 0–5 scoring system for each independent parameter.

Serum Biomarker Analysis

Serum biomarkers of kidney and liver function were analyzed using an Ortho Vitros 5.1 Chemistry Analyzer by the Iowa State University Clinical Pathology Laboratory. Toxicological biomarkers analyzed included blood urea nitrogen (BUN), albumin, alkaline phosphatase (Alk Phos), alanine aminotransferase (ALT), serum creatinine, glucose, total bilirubin, cholesterol, and total triglycerides. Normal range values for these biomarkers were obtained from the Laboratory and compared with those in the literature (34,35).

Urine Creatinine and Total Protein Quantification Analysis

Creatinine levels were measured in urine samples collected at 7 and 30 days post-administration using a creatinine assay kit (Sigma-Aldrich). The ELISA-based colorimetric assay was performed following the manufacturer's specifications. Quantification of creatinine was performed using standards provided by the manufacturer. Total protein amount in urine was quantified using a micro-bicinchoninic acid (BCA) assay at an absorbance of 562 nm using a plate reader (SpectraMax M3).

Intranasal Administration of Particle Formulations

Five separate groups of Swiss Webster mice were intranasally administered with nanoparticle formulations. To sedate the mice prior to intranasal administration of the nanoparticles, the mice were intraperitoneally injected with 90 μ L of anesthetic solution (20 mg/mL ketamine + 1 mg/mL xylazine). Particle treatment groups included mice that were administered with the following: (1) 500 μ g of nonfunctionalized, (2) linker-functionalized, (3) galactose-functionalized, or (4) di-mannose-functionalized 50:50

CPTEG:CPH nanoparticles. Mice intranasally administered with saline were used as a control. Nanoparticles were suspended in PBS and sonicated before administration. For all formulations, a volume of 50 μ L was intranasally administered. After mice were deeply anesthetized, they were held upright by the nape of the neck and nanoparticle suspension was slowly applied through the nostrils of each mouse with a micropipette. They were held in this position until the breathing rate of the animals was back to normal. Mice were monitored after anesthesia and mobile function was restored.

Lung Histological Evaluation

Lungs from Swiss Webster mice were excised at 6, 24, and 48 h post-immunization and formalin-fixed. Tissues were embedded, sectioned, and stained with H&E and blindly evaluated by a board-certified veterinary pathologist. Adverse reactions in the lung tissue caused by inflammatory infiltration, necrosis, edema, bronchial associated lymphoid tissue (BAL) hyperplasia, and hemorrhage were evaluated using a 0–5 scoring system for each independent parameter.

Flow Cytometric Analysis of Lung Tissue

Mice were euthanized at 2, 24, and 48 h time points post-immunization. Lungs were processed as previously described (9). Briefly, lungs were excised and perfused with PBS. Lungs were incubated in Hank's Balanced Salt Solution with 1 mg/mL collagenase D and 60 U/mL DNase II for 20 min at 37°C. Lung tissue was homogenized using a gentleMACS® tissue dissociator (Miltenyi Biotec, Cambridge, MA). To remove debris, samples were centrifuged for 250 rcf for 20 s and filtered with a 40- μ m-cell filter. Red blood cells were lysed using ACK lysis buffer (150 mM ammonium chloride, 10 mM potassium bicarbonate, and 0.1 mM EDTA). Cell samples (1×10^6 cells/mL) were blocked to prevent nonspecific binding with 1% Rat IgG, 0.1% anti-mouse CD16/32, and 0.1% unconjugated Armenian Hamster IgG. Cells were surface stained with CD11c, CD11b, Ly6G/C Gr-1, and F4/80 markers. Samples were fixed with a stabilizing fixative solution (BD Biosciences) and analyzed on a FACSCanto™ flow cytometer (Becton-Dickinson, San Jose, CA), and the data was processed using FlowJo vX software (TreeStar Inc., Ashland, OR).

Bronchoalveolar Lavage Fluid Collection

Bronchoalveolar lavage (BAL) fluid was collected at 6, 24, and 48 h post-immunization (36,37). Briefly, after mice were euthanized, a sterile catheter was inserted into the exteriorized trachea of each mouse. Using a 1-mL syringe attached to the catheter, 1 mL of PBS was infused into the lungs and aspirated back to the syringe. The process was repeated two to three times, per mouse, while massaging the chest externally. Samples were placed on ice and centrifuged at 300 rcf for 30 s at RT to remove cellular debris and stored at -20°C until further analysis.

Cytokine and Chemokine Analysis

BAL fluid samples obtained at 6, 24, and 48 h post-immunization were analyzed using a 13-plex cytokine and chemokine quantification kit (MILLIPLEX® MAP Mouse Cytokine/Chemokine Magnetic Bead Panel, EMD Millipore, Billerica, MA). Analytes quantified included interleukin 6 (IL-6), keratinocyte chemoattractant (KC), monocyte chemoattractant protein 1 (MCP-1), macrophage inflammatory protein 1 α (MIP-1 α), macrophage inflammatory protein 2 (MIP-2), IFN-inducible protein 10 (IP-10), tumor necrosis factor alpha (TNF- α), interferon gamma (IFN- γ), interleukin 1 β (IL-1 β), interleukin 10 (IL-10), interleukin 12p40 (IL-12p40), monokine induced by IFN- γ (MIG), and regulated on activation, normal T cell expressed and secreted (RANTES). The assay was performed following the manufacturer's instructions, and data was acquired and analyzed using a Bio-Plex 200™ system (Bio-Rad, Hercules, CA) as described in previous protocols (8,17).

Statistical Analysis

Statistical analysis was used to analyze the cell surface marker expression and cytokine secretion data. Two-way ANOVA and Dunnett's test were used to determine statistical significance among treatments, and *p* values <0.05 were considered significant.

RESULTS

Functionalization and Characterization of Carbohydrate-Modified Nanoparticles

Our previous work has shown that amphiphilic nanoparticle chemistries were suitable for protein stabilization (16,24,28,38,39), demonstrated potent adjuvant responses (20), and were effectively internalized by and activated APCs (6,17,24,40). Therefore, the 50:50 CPTEG:CPH nanoparticle formulation was chosen to perform the carbohydrate functionalization and to evaluate safety upon *in vivo* administration.

Particle morphology was characterized using scanning electron microscopy, as shown by the photomicrographs in Fig. 1. The size of these particles was measured using ImageJ software (version 1.47v, NIH, Bethesda, MD). The diameter of the nonfunctionalized 50:50 CPTEG:CPH nanoparticles was 182 ± 59 nm. After functionalization, the diameter increased to 223 ± 61 , 228 ± 43 , and 236 ± 55 nm, for linker-, galactose-, and di-mannose-modified particles, respectively. In addition, the ζ -potentials and the surface concentration of the sugars for each formulation were measured and are shown in Fig. 1. The NF particles are negatively charged, consistent with the presence of carboxylic acid moieties with a ζ -potential of -21 ± 3.2 mV, while the addition of the amine linker to which the neutral sugar moieties (*i.e.*, galactose and di-mannose) were attached resulted in a positively charged surface with ζ -potentials of 18 ± 2.5 , 16 ± 2.1 , and 19 ± 1.9 mV, respectively. After the carbohydrate modification was completed, quantification of the amount of sugar linked to the particle surface was measured using a phenol-sulfuric acid

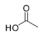
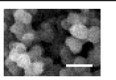
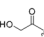
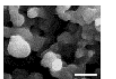
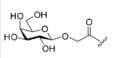
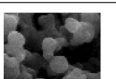
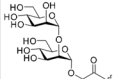
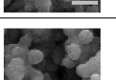
Nanoparticle type	Structure of surface moiety	SEM photomicrographs (scale bar: 500 nm)	Average particle diameter (nm)	Average ζ potential (mV)	Sugar density ($\mu\text{g}/\text{mg}$ of particles)
Non-functionalized			182 \pm 59	-21 \pm 3.2	N/A
Linker functionalized			223 \pm 61	18 \pm 2.5	N/A
Galactose functionalized			228 \pm 43	16 \pm 2.1	15 \pm 5.5
Di-mannose functionalized			236 \pm 55	19 \pm 1.9	19 \pm 2.4

Fig. 1. Polyanhydride nanoparticle characterization. Chemical structures of the surface moieties on nonfunctionalized and linker-, galactose-, and di-mannose-functionalized nanoparticles are presented. Particle size data represent the mean \pm standard deviation (SD) of data collected from scanning electron microscopy photomicrographs using ImageJ software from four independent experiments. ζ -potential data were measuring using QELS and represent the mean \pm SD of four independent experiments. Sugar density data were measured using a phenol sulphuric acid assay and are presented as the mean \pm SD of four independent experiments

assay and indicated that 15 \pm 5.5 μg of galactose or 19 \pm 2.4 μg of di-mannose was present per milligram of particles.

Kidney Histological Evaluation and Renal Function

Following subcutaneous administration of 5 mg of particles to mice, serum, urine, and kidney samples were collected at 7 and 30 days. Histological evaluation of the tissue sections was performed, and renal function biomarker levels were analyzed. Blood urea nitrogen (BUN) was measured in serum samples, while creatinine and total protein were quantified in urine samples. As shown in the representative histological images in Fig. 2a, the inflammatory changes in the kidney during the period of the study were unremarkable as no significant differences were observed between the histological scores of mice treated with saline and the animals treated with the various nanoparticle formulations. Using a 5-point scale, the inflammatory infiltration scores ranged from 0 to 2, in all groups, with an average of 0.67, and these levels did not worsen between 7 and 30 days postadministration, indicating that no acute or chronic inflammation was induced (Fig. 2b). The distribution of the cellular infiltration had an average score of \sim 1.67, with only one mouse that was administered with galactose nanoparticles receiving a score of 3 at 7 days postadministration. In summary, these studies show that there was no histological evidence of tissue damage in the kidneys. Figure 2c shows renal function biomarker levels, BUN, and creatinine, both indicative of normal glomerular filtration rate. For the two biomarkers assessed and the total protein/creatinine ratio in the urine, there were no significant differences in urine samples collected at 7 or

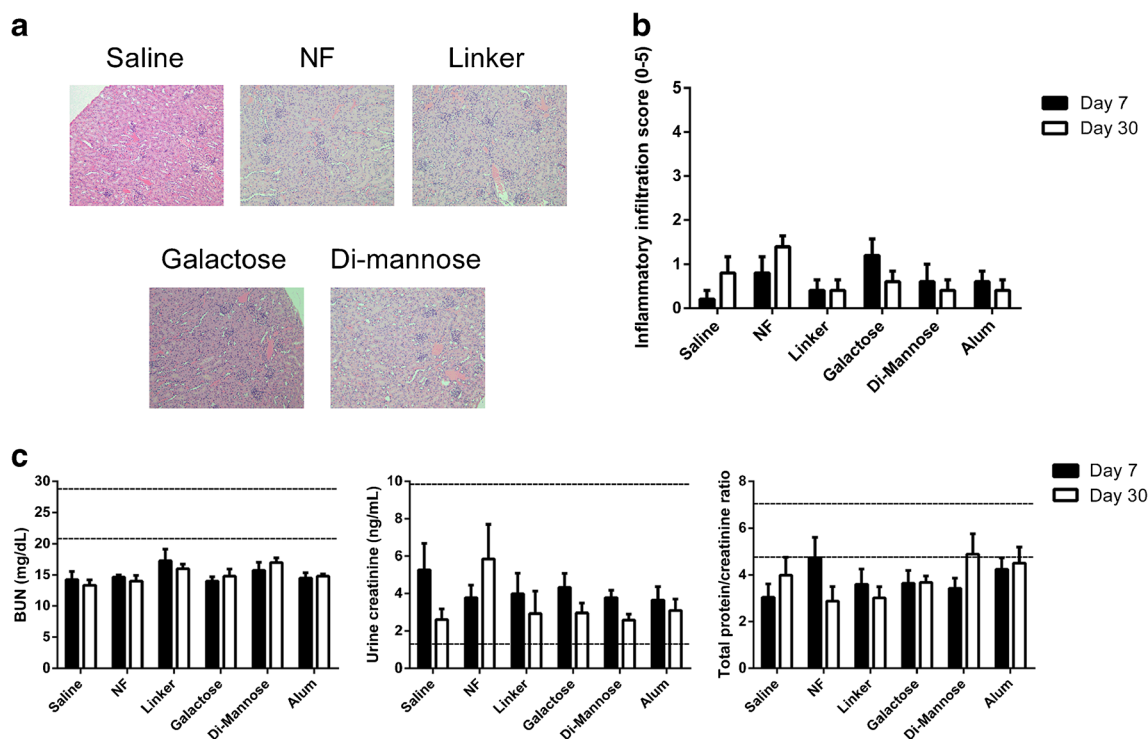


Fig. 2. Administration of a 5-mg dose of surface-functionalized 50:50 CPTEG:CPH nanoparticles did not affect renal function. Panel a shows representative histological sections of kidney samples from Swiss Webster mice ($n=6$) 7 days post-administration of the nanoparticle formulations. Panel b shows the inflammatory scores of kidney samples after histopathological evaluation. Panel c displays the levels of blood urea nitrogen (BUN) in serum and creatinine and total protein/creatinine ratio in urine samples from Swiss Webster mice 7 and 30 days post-administration. Reference levels provided by the Iowa State University Clinical Pathology Laboratory are indicated as dashed lines. No significant differences were observed when compared to mice administered with saline ($n=5$ at each time point)

30 days post-administration from mice that were treated with saline and samples from mice that received any of the nanoparticle treatments. Both BUN and creatinine levels were within previously reported normal range levels (41,42). Even though BUN levels were slightly lower than the reference values, there were no significant differences between the saline and particle groups. Variations in normal BUN levels have been previously reported to be mouse strain-dependent (34,35,43).

Liver Histological Evaluation and Hepatic Function

Histological evaluation of the tissue sections was performed, 7 and 30 days after subcutaneous administration of 5 mg of nanoparticle formulations. Cholestasis and hepatocellular damage were evaluated in serum samples by measuring the levels of Alk Phos and ALT, respectively. As shown in Fig. 3a, the inflammatory changes in the liver were mild, and these were interpreted as nonspecific background changes common to this mouse strain. Representative histological images of liver tissue are shown. The inflammatory infiltration scores ranged from 0 to 2 (on a scale of 0–5) in all the animals studied, with an average of ~1, regardless of the treatment as shown in Fig. 3b. These scores did not significantly change between the two time points analyzed. The frequency of infiltration within the liver (distribution score) was also low; the distribution score ranged from 0 to 3, with an average of ~1.8. In Fig. 3c, the levels of Alk Phos, ALT, and albumin are shown. There were no significant differences in the serum

levels of any of the biomarkers analyzed between saline and nanoparticle treatment groups in the levels of these serum biomarkers at either time point. The ALT levels in mice administered with particle formulations were slightly higher than the upper limit of the reference values at day 30 post-administration; however, these were no different than the levels observed in mice treated with saline at the same time point.

Lung Histological Evaluation

Based upon the results obtained so far, which suggested that the subcutaneous administration of carbohydrate-functionalized polyanhydride nanoparticles did not have a detrimental effect upon liver or kidney function of the treated animals, we next evaluated the safety profile upon intranasal administration of surface-modified polyanhydride nanoparticles. Previous work from our laboratories has shown that nanovaccines delivered intranasally resulted in protective long-term immunity (20). After intranasal administration of 0.5 mg of nanoparticle formulations, tissue samples were collected at 6, 24, and 48 h postadministration to evaluate acute histological changes. Figure 4a shows representative histological images from the lung for each treatment group at the 24-h time point (when the highest histological scores were registered). The parameter that contributed mostly to the final histological score was inflammation as shown in Fig. 4b. Inflammatory infiltrates tended to be focused on bronchioles and adjacent alveolar spaces with neutrophils predominating.

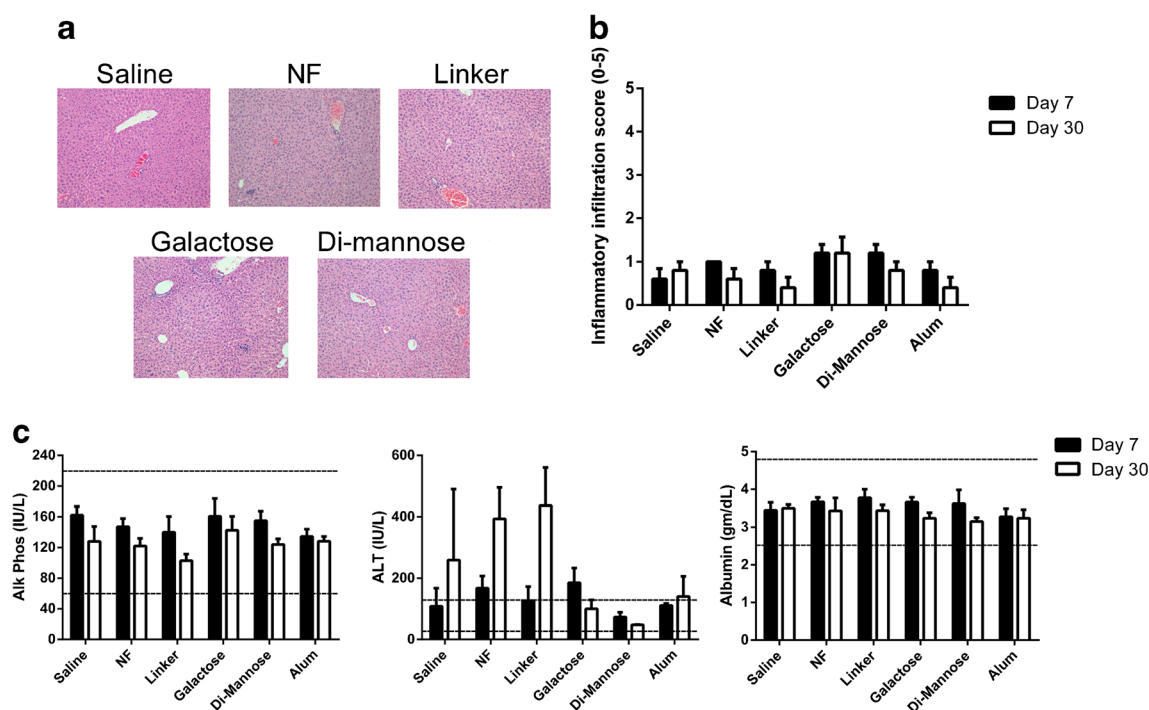


Fig. 3. Administration of a 5-mg dose of surface-functionalized 50:50 CPTEG:CPH nanoparticles did not affect hepatic inflammation or alter hepatic function. Panel a shows representative histological sections of liver samples from Swiss Webster mice ($n=6$) 7 days post-administration of the nanoparticle formulations. Panel b shows the inflammatory scores of liver samples after histopathological evaluation. Panel c displays the levels of alkaline phosphatase, alanine aminotransferase, and albumin in serum samples from Swiss Webster mice 7 and 30 days post-administration. Reference levels provided by the Iowa State University Clinical Pathology Laboratory are indicated as dashed lines. No significant differences were observed when compared to mice administered with saline ($n=5$ at each time point)

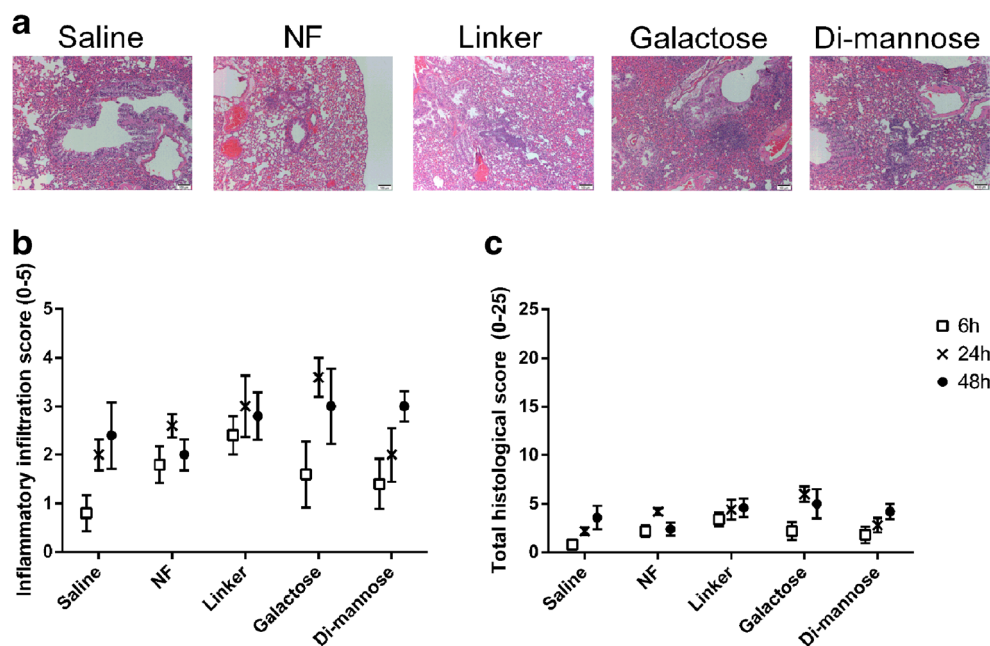


Fig. 4. Mild-to-moderate inflammation was observed in lung samples upon histological evaluation post-administration of surface-functionalized polyanhydride nanoparticles. Lung tissue samples from Swiss Webster mice were collected at 6, 24, and 48 h post-administration. **a** Representative images of each treatment group at 24 h post-administration. **b** Inflammatory infiltration scores on a scale of 0–5 after histopathological evaluation. **c** Composite histopathological scores representing the sum of five individual parameters (inflammatory infiltration, necrosis, edema, bronchial associated lymphoid tissue hyperplasia, and hemorrhage), with a total possible score of 25. No significant differences were observed when compared to mice administered with saline ($n=6$ at each time point)

In general, the inflammatory scores peaked at 24 h, with scores up to 4 in some animals. The animals that received the linker- and galactose-functionalized nanoparticles displayed a higher level of inflammation. In addition, the average necrosis values increased with time, with the highest value at 48 h, regardless of the treatment groups (data not shown). There were only two mice with minor hemorrhage, with a score of 1, 24 h after administration of the NF particles. Hemorrhage was likely a tissue collection artifact. There were no mice with signs of edema or BALT hyperplasia at any time point analyzed (data not shown). Total histological scores are shown in Fig. 4c.

Distribution of Lung Cellular Populations

Given the inflammatory cell infiltration scores described above, the cell types recruited into the lungs following particle administration were assessed by flow cytometry. Cellular populations were analyzed in whole-lung homogenate at 2, 24, and 48 h post-intranasal administration. Flow cytometric analysis was performed, and populations were identified with the following surface marker combinations: dendritic cells ($CD11c^+ CD11b^-$), interstitial macrophages ($CD11c^- CD11b^+ F4/80^+$), neutrophils ($CD11b^+ Ly6G/C Gr-1^+$), and activated monocytes ($CD11b^+ Ly6G/C Gr-1^-$) (44–47). Figure 5 shows the cellular population distribution in the lungs. The percentage of DCs (Fig. 5a) increased with time for all the treatment groups including the saline control and ranged from 1% to 4% of total lung cells. The percentage of interstitial macrophages (Fig. 5b) peaked at 24 h, with all the treatment groups following similar dynamics. The neutrophil

percentage (Fig. 5c) at 2 h was the highest (2.5%–5%), and with time, these populations decreased to 1.5%–2.5% of all the cells; this behavior was observed in the tissue from the animals that received all the treatment groups except the NF nanoparticles, in which the neutrophil population peaked at 24 h. As another measure of cellular recruitment into the lungs, the presence of activated monocytes was assessed (Fig. 5d) and the presence of this cell type followed similar dynamics as neutrophils, starting at 4%–6% and decaying to 1.5%–3% of total lung cells by 48 h. These data support the histological evaluation, as no major changes were observed in the inflammatory cell populations in the lungs of mice treated with saline or mice administered with any of the nanoparticle formulations.

Cytokine/Chemokine Secretion

To assess the inflammatory environment in the lungs following intranasal administration of 0.5 mg of nanoparticle formulations, the BAL fluid was collected and used to measure the amounts of the following chemokines and cytokines: IL-6, KC, MCP-1, MIP-1 α , MIP-2, IP-10, TNF- α , IFN- γ , IL-1 β , IL-10, IL-12p40, MIG, and RANTES. Negligible amounts (*i.e.*, below the levels of detection) of IFN- γ , IL-1 β , IL-10, IL-12p40, MIG, and RANTES were observed (data not shown). Figure 6 shows the kinetics of the secretion of IL-6, KC, MIP-2, TNF- α , IP-10, MCP-1, and MIP-1 α . Two distinct trends were observed. The secretion of IL-6, KC, MIP-2, and TNF- α peaked at 6 h postadministration, while the highest amounts of IP-10, MCP-1, and MIP-1 α secreted were observed 48 h postadministration. The BAL fluid from

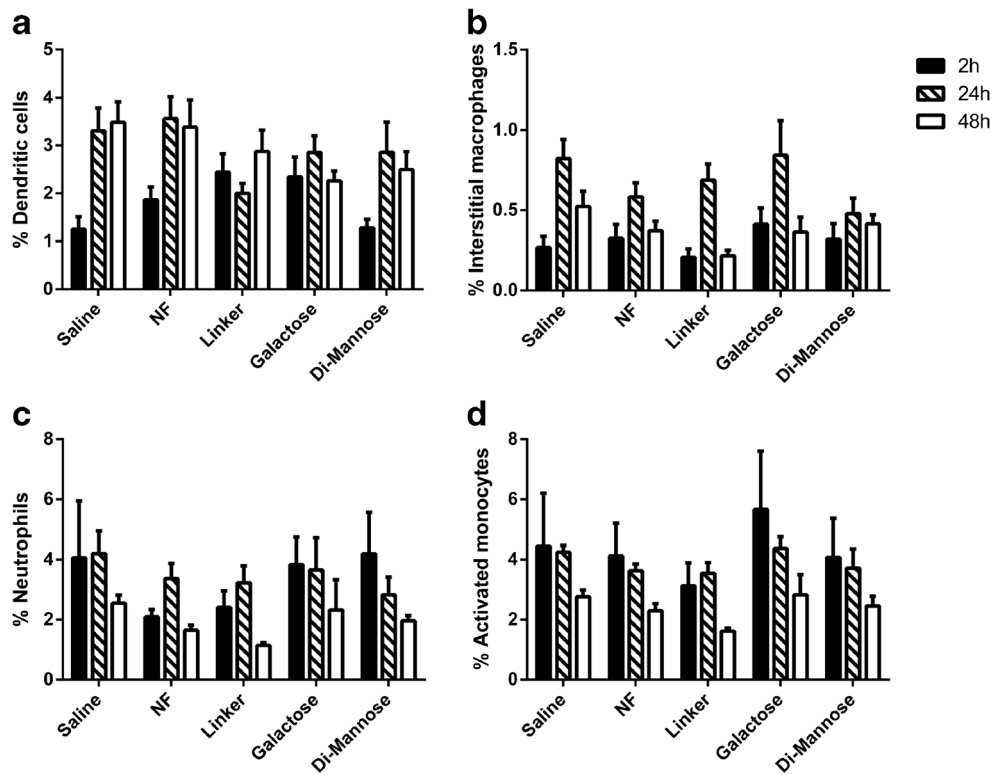


Fig. 5. Cellular distribution of lung homogenates of Swiss Webster following administration of surface-functionalized polyanhydride nanoparticles. Cellular populations were analyzed by flow cytometry at 6, 24, and 48 h post-administration, and various cell populations were analyzed. **a** dendritic cells, **b** interstitial macrophages, **c** neutrophils, and **d** activated monocytes. No significant differences were observed in these distributions when compared to mice administered with saline ($n=6$ at each time point)

animals that received the linker- and galactose-modified nanoparticle groups showed consistently higher amounts of these cytokines compared with saline. The absence of a major cytokine/chemokine response after intranasal administration of the nanoparticle formulations is consistent with the histological data and provides further evidence of the safety and biocompatibility of these materials following pulmonary delivery.

DISCUSSION

In this work, we report on the safety profile of surface-functionalized polyanhydride nanoparticles following parenteral or intranasal administration to mice. The safety and biocompatibility of nonfunctionalized polyanhydride nanoparticles has been demonstrated previously (33); however, the ability of di-mannose-functionalized nanoparticles to initiate

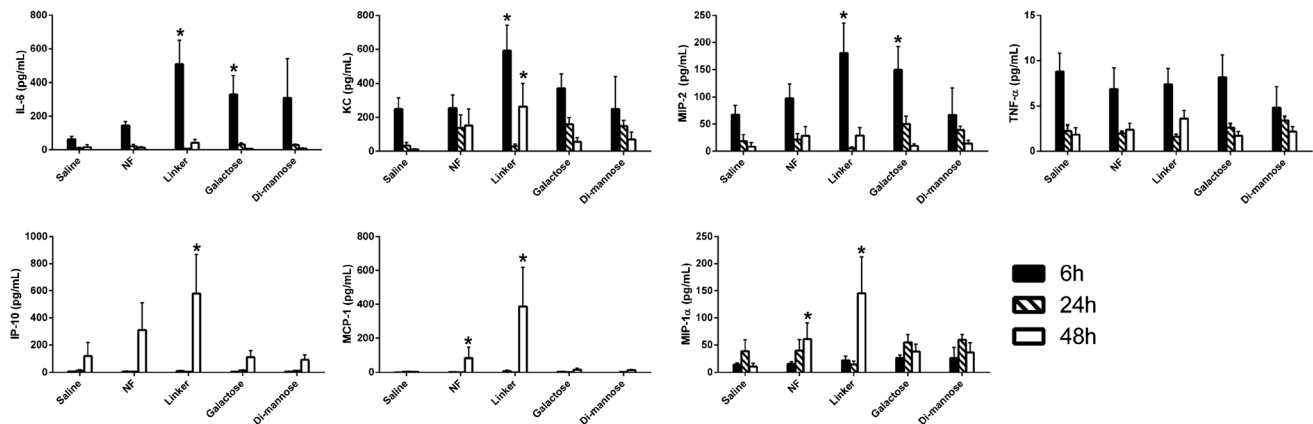


Fig. 6. Low amounts of cytokine/chemokine secretion were observed in bronchoalveolar lavage fluid 6, 24, and 48 h after intranasal administration of surface-functionalized polyanhydride nanoparticles. The amounts of IL-6, KC, MIP-2, TNF- α , IP-10, MCP-1, and MIP-1 α in the bronchoalveolar lavage fluid were quantified using a multiplex magnetic bead assay. Asterisk represents groups that are statistically significant ($p \leq 0.05$) compared to the saline control ($n=5$ at each time point)

signaling *via* CLRs warrants a systematic evaluation of the potential toxicity associated with the induction of innate and/or inflammatory responses by these novel biomaterials.

As shown in Fig. 1, the particle morphology and size of the functionalized particles were similar to previously reported data (6,19,28,48,49). The characterization of polyanhydride nanoparticles before and after surface modification was consistent with previous studies (6,17,18). The change in the ζ -potential from negative to positive charge after linker attachment can be beneficial for enhanced cellular uptake, as reported previously (50,51). In addition, carbohydrate functionalization is known to enhance both the APC activation *in vitro* (6,17,18) and the therapeutic efficacy of drug delivery (4).

Based on the histological analysis scores reported in this work, subcutaneous administration of 5 mg of carbohydrate-functionalized nanoparticles did not result in tissue damage of the liver or kidney when assessed at 7 or 30 days postadministration and is consistent with previously reported safety profiles of parenterally administered polyanhydride nanoparticles (33). The histological changes noted in hepatic tissue samples after nanoparticle administration were mild, which are comparable to other biodegradable polymer formulations, but much less than those exhibited by extremely cytotoxic metal particles of similar size (11). No other histological changes such as distortion and swelling of hepatocytes, cellular binucleation, or hydropic degeneration of the tissue were detected in the liver samples, as reported with other nanoparticle formulations (52). The histological scores of the kidney samples of mice administered with saline alone were not significantly different when compared to the scores from the kidneys of mice administered with various particle formulations. No interstitial edema, inflammatory cell infiltration, tubular epithelial flattening, urinary casts, or signs of renal histopathological lesions were detected, which have been reported previously for other nanoparticles (53,54). Based on the data presented here, the systemic effects of functionalized nanoparticle administration, in terms of hepatic and renal health, are consistent with the effects of other biodegradable nanoparticle systems (33,55,56).

In addition to histological evaluation, serum and urine biomarkers, which are indicators of renal and hepatic injury and inflammation, were used to evaluate the safety of the functionalized nanoparticles. The levels of BUN, urine creatinine, and total protein/creatinine ratio in mice receiving the particle treatments were not significantly different from the levels in animals receiving the saline. Even though BUN content level was lower than the reference values provided, the values were consistent with previously reported data in Swiss Webster mice (43). Creatinine and total protein-to-creatinine ratio levels in mice administered with the particles were no different than in animals receiving the saline control and consistent with the amounts reported in urine from mice of this lineage (35,41). Creatinine, a by-product of muscle metabolism, is an important indicator of kidney function. When glomerular filtration rate is impaired, creatinine levels rise in the blood and in the urine (57). Creatinine measurement is commonly used because urinary excretion of any biomarker that is filtered through the glomerulus is affected by the glomerular filtration rate and therefore used to normalize other markers, such as total protein or albumin

(58). Together with urine specific gravity, these markers are part of the standard clinical diagnosis for renal function during impairments such as chronic kidney disease (59), acute kidney injury (60), or renal injury (41). Together, the inability to detect elevated levels of key biomarkers in serum and urine, combined with the histopathology assessment of liver and kidney samples, demonstrates that there were no detrimental effects on renal or hepatic systems in mice treated with 5 mg of di-mannose-functionalized nanoparticles.

The use of the pulmonary route offers several advantages for drug and vaccine delivery since the lungs allow targeted (2), noninvasive administration (22) and the capability to ensure systemic or local delivery of agents (12,21). However, the respiratory system is also a more delicate environment, and parameters such as particle size (61–63), charge (2,50,51), chemistry (9,33), and material (12,64) affect deposition, distribution, and biocompatibility. In previous work, a single intranasal administration of nonfunctionalized polyanhydride nanovaccines demonstrated the ability to induce protective immunity upon lethal challenge (9,20,65). The current work builds upon these studies by evaluating the safety profile of carbohydrate-functionalized nanoparticles in the lung. The acute histopathology results from lung tissues after administration of particle formulations (Fig. 4) displayed a bell-shaped curve with a peak at the 24-h time point. The lesions in the lung samples were mild to moderate, likely attributable to the administration procedure itself, because the lungs of the mice administered with the saline control group received similar scores. As shown in Fig. 4b, the major contributor to the histological scores was inflammatory cell infiltration.

The inflammatory infiltrates found in the lung samples after intranasal administration were consistent with the recruitment kinetics described for other pulmonary innate immune responses (36,50,61,66), in which initial cellular recruitment was primarily composed of mononuclear cells and neutrophils. Next, neutrophils and macrophage infiltrates appeared in the lung tissue by 24 h and were still present 48 h post-administration. Since the differences in the inflammatory cell infiltrates in the lung samples may be attributed to pulmonary recruitment of cells from circulation (50), we analyzed the kinetics of various cell populations in the lungs of treated animals. As shown in Fig. 5, there were no significant changes in lung cellular populations between the various particle treatment groups, but all of them followed similar kinetics. Consistent with the histological data and previous studies (66,67), neutrophils were the first cells to be recruited to the administration site, followed by macrophages and/or DCs. Overall, the lung cellular populations observed were not statistically distinguishable from the populations in the lungs of mice receiving saline. This observation suggests that the administration of the nanoparticles likely caused a mild inflammatory response similar to that induced by the administration of saline, and supports the conclusion that the particle formulations themselves were not detrimental to the health of the treated animals.

Another component of lung response to foreign material is the secretion of cytokines and chemokines to recruit a cellular response and mediate clearance. The presence of these molecules can mediate leukocyte trafficking and inflammation and link the innate and adaptive immune responses (68). However, overproduction of chemokines and

cytokines can cause severe tissue damage (68,69). As shown in Fig. 6, different kinetics were observed for the analyzed cytokines and chemokines. The amounts of IL-6, KC, MIP-2, and TNF- α levels were elevated at early time points but decreased by 48 h, while the amounts of IP-10, MCP-1, and MIP-1 α secreted were the highest at 48 h. The observed differential production of these cytokines/chemokines is likely related to the dynamic nature of the innate immune response and the different cell types that produce, utilize, and respond to these molecules. Nevertheless, our data indicate that intranasal administration of any of the nanoparticle formulations did not cause a major increase in cytokine or chemokine production that would result in severe tissue damage. All together, the histological evaluation of lung tissue, the unremarkable changes in the recruitment of inflammatory cells to the lung, and the absence of a major cytokine/chemokine response after intranasal administration of carbohydrate-functionalized polyanhydride nanoparticles provide confirmatory evidence of the safety and biocompatibility of these novel materials for pulmonary delivery.

CONCLUSIONS

The studies reported herein demonstrate the safety and biocompatibility of carbohydrate-functionalized polyanhydride nanoparticles upon parenteral and intranasal administration. The results showed that a 5-mg dose of either linker- or di-mannose-functionalized nanoparticles did not induce hepatic or renal tissue damage or cause elevation of damage-related or functional biomarkers in serum or urine following subcutaneous administration. In addition, a 0.5-mg dose of either linker- or di-mannose-functionalized nanoparticles administered intranasally did not result in demonstrable tissue changes in the lungs of treated animals. The favorable histological profile, the distribution and kinetics of cellular populations, and the lack of a remarkable pro-inflammatory cytokine and chemokine profile in the lungs of mice administered with functionalized nanoparticles supported the biocompatibility of the linker- and di-mannose-functionalized nanoparticles. Together, these studies demonstrate the safety of administering carbohydrate-functionalized nanoparticles *in vivo* and provide foundational information to evaluate the capabilities of these surface-modified nanoparticles for drug and vaccine delivery.

ACKNOWLEDGMENTS

The authors would like to acknowledge the financial support from NIH-NIAID (U19 AI-091031) and U.S. Army Medical Research and Materiel Command (grant no. W81XWH-10-1-0806). The authors would also like to thank Shawn Rigby of the ISU Flow Cytometry Facility for his expertise in flow cytometry.

REFERENCES

- Engering A, Geijtenbeek TB, van Vliet SJ, Wijers M, van Liempt E, Demarex N, *et al.* The dendritic cell-specific adhesion receptor DC-SIGN internalizes antigen for presentation to T cells. *J Immunol.* 2002;168(5):2118–26.
- Azarmi S, Roa WH, Lobenberg R. Targeted delivery of nanoparticles for the treatment of lung diseases. *Adv Drug Deliv Rev.* 2008;60(8):863–75.
- Geijtenbeek TB, Gringhuis SI. Signalling through C-type lectin receptors: shaping immune responses. *Nat Rev Immunol.* 2009;9(7):465–79.
- Irache JM, Salman HH, Gamazo C, Espuelas S. Mannose-targeted systems for the delivery of therapeutics. *Expert Opin Drug Deliv.* 2008;5(6):703–24.
- Ulery BD, Nair LS, Laurencin CT. Biomedical applications of biodegradable polymers. *J Polym Sci B Polym Phys.* 2011;49(12):832–64.
- Carrillo-Conde B, Song EH, Chavez-Santoscoy A, Phanse Y, Ramer-Tait AE, Pohl NL, *et al.* Mannose-functionalized “pathogen-like” polyanhydride nanoparticles target C-type lectin receptors on dendritic cells. *Mol Pharm.* 2011;8(5):1877–86.
- Torres MP, Wilson-Welder JH, Lopac SK, Phanse Y, Carrillo-Conde B, Ramer-Tait AE, *et al.* Polyanhydride microparticles enhance dendritic cell antigen presentation and activation. *Acta Biomater.* 2011;7(7):2857–64.
- Petersen LK, Xue L, Wannemuehler MJ, Rajan K, Narasimhan B. The simultaneous effect of polymer chemistry and device geometry on the *in vitro* activation of murine dendritic cells. *Biomaterials.* 2009;30(28):5131–42.
- Ross KA, Haughney SL, Petersen LK, Boggianto P, Wannemuehler MJ, Narasimhan B. Lung deposition and cellular uptake behavior of pathogen-mimicking nanovaccines in the first 48 hours. *Adv Healthc Mater.* 2014;3(7):1071–7.
- Carrillo-Conde BR, Ramer-Tait AE, Wannemuehler MJ, Narasimhan B. Chemistry-dependent adsorption of serum proteins onto polyanhydride microparticles differentially influences dendritic cell uptake and activation. *Acta Biomater.* 2012;8(10):3618–28.
- Semete B, Booyesen L, Lemmer Y, Kalombo L, Katata L, Verschoor J, *et al.* *In vivo* evaluation of the biodistribution and safety of PLGA nanoparticles as drug delivery systems. *Nanomedicine.* 2010;6(5):662–71.
- Mansour HM, Rhee YS, Wu X. Nanomedicine in pulmonary delivery. *Int J Nanomedicine.* 2009;4:299–319.
- Nguyen J, Steele TW, Merkel O, Reul R, Kissel T. Fast degrading polyesters as siRNA nano-carriers for pulmonary gene therapy. *J Control Release.* 2008;132(3):243–51.
- Torres MP, Determan AS, Anderson GL, Mallapragada SK, Narasimhan B. Amphiphilic polyanhydrides for protein stabilization and release. *Biomaterials.* 2007;28(1):108–16.
- Torres MP, Vogel BM, Narasimhan B, Mallapragada SK. Synthesis and characterization of novel polyanhydrides with tailored erosion mechanisms. *J Biomed Mater Res A.* 2006;76(1):102–10.
- Carrillo-Conde B, Schiltz E, Yu J, Chris Minion F, Phillips GJ, Wannemuehler MJ, *et al.* Encapsulation into amphiphilic polyanhydride microparticles stabilizes *Yersinia pestis* antigens. *Acta Biomater.* 2010;6(8):3110–9.
- Chavez-Santoscoy AV, Roychoudhury R, Pohl NL, Wannemuehler MJ, Narasimhan B, Ramer-Tait AE. Tailoring the immune response by targeting C-type lectin receptors on alveolar macrophages using “pathogen-like” amphiphilic polyanhydride nanoparticles. *Biomaterials.* 2012;33(18):4762–72.
- Vela Ramirez JE, Roychoudhury R, Habte HH, Cho MW, Pohl NL, Narasimhan B. Carbohydrate-functionalized nanovaccines preserve HIV-1 antigen stability and activate antigen presenting cells. *J Biomater Sci Polym Ed.* 2014;25(13):1387–406.
- Huntimer LM, Ross KA, Darling RJ, Winterwood NE, Boggianto P, Narasimhan B, *et al.* Polyanhydride nanovaccine platform enhances antigen-specific cytotoxic T cell responses. *Technology.* 2014;02(02):171–5.
- Ulery BD, Kumar D, Ramer-Tait AE, Metzger DW, Wannemuehler MJ, Narasimhan B. Design of a protective single-dose intranasal nanoparticle-based vaccine platform for respiratory infectious diseases. *PLoS One.* 2011;6(3):e17642.
- Patton JS, Byron PR. Inhaling medicines: delivering drugs to the body through the lungs. *Nat Rev Drug Discov.* 2007;6(1):67–74.

22. Sung JC, Pulliam BL, Edwards DA. Nanoparticles for drug delivery to the lungs. *Trends Biotechnol.* 2007;25(12):563–70.
23. Bailey MM, Berkland CJ. Nanoparticle formulations in pulmonary drug delivery. *Med Res Rev.* 2009;29(1):196–212.
24. Phanse Y, Carrillo-Conde BR, Ramer-Tait AE, Roychoudhury R, Pohl NL, Narasimhan B, *et al.* Functionalization of polyanhydride microparticles with di-mannose influences uptake by and intracellular fate within dendritic cells. *Acta Biomater.* 2013;9(11):8902–9.
25. Napoletano C, Zizzari IG, Ruggetti A, Rahimi H, Irimura T, Clausen H, *et al.* Targeting of macrophage galactose-type C-type lectin (MGL) induces DC signaling and activation. *Eur J Immunol.* 2012;42(4):936–45.
26. Cambi A, Figdor CG. Dual function of C-type lectin-like receptors in the immune system. *Curr Opin Cell Biol.* 2003;15(5):539–46.
27. Conix A. Poly[1,3-bis(*p*-carboxyphenoxy)-propane anhydride]. *Macro Synth.* 1966;2:95–8.
28. Ulery BD, Phanse Y, Sinha A, Wannemuehler MJ, Narasimhan B, Bellaire BH. Polymer chemistry influences monocytic uptake of polyanhydride nanospheres. *Pharm Res.* 2009;26(3):683–90.
29. Curran DP, Luo Z. Fluorous synthesis with fewer fluorines (light fluorine synthesis): separation of tagged from untagged products by solid-phase extraction with fluorine reverse-phase silica gel. *J Am Chem Soc.* 1999;121(39):9069–72.
30. Zhang W, Curran DP. Synthetic applications of fluorine solid-phase extraction (F-SPE). *Tetrahedron.* 2006;62(51):11837–65.
31. Zhang W. Fluorous linker-facilitated chemical synthesis. *Chem Rev.* 2009;109(2):749–95.
32. Masuko T, Minami A, Iwasaki N, Majima T, Nishimura S, Lee YC. Carbohydrate analysis by a phenol-sulfuric acid method in microplate format. *Anal Biochem.* 2005;339(1):69–72.
33. Huntimer L, Ramer-Tait AE, Petersen LK, Ross KA, Walz KA, Wang C, *et al.* Evaluation of biocompatibility and administration site reactivity of polyanhydride-particle-based platform for vaccine delivery. *Adv Healthc Mater.* 2013;2(2):369–78.
34. Mazzaccara C, Labruna G, Cito G, Scarfo M, De Felice M, Pastore L, *et al.* Age-related reference intervals of the main biochemical and hematological parameters in C57BL/6J, 129SV/EV and C3H/HeJ mouse strains. *PLoS One.* 2008;3(11):e3772.
35. Cheetham SA, Smith AL, Armstrong SD, Beynon RJ, Hurst JL. Limited variation in the major urinary proteins of laboratory mice. *Physiol Behav.* 2009;96(2):253–61.
36. Kirby AC, Raynes JG, Kaye PM. CD11b regulates recruitment of alveolar macrophages but not pulmonary dendritic cells after pneumococcal challenge. *J Infect Dis.* 2006;193(2):205–13.
37. Kirby AC, Coles MC, Kaye PM. Alveolar macrophages transport pathogens to lung draining lymph nodes. *J Immunol.* 2009;183(3):1983–9.
38. Kipper MJ, Shen E, Determan A, Narasimhan B. Design of an injectable system based on bioerodible polyanhydride microspheres for sustained drug delivery. *Biomaterials.* 2002;23(22):4405–12.
39. Lopac SK, Torres MP, Wilson-Welder JH, Wannemuehler MJ, Narasimhan B. Effect of polymer chemistry and fabrication method on protein release and stability from polyanhydride microspheres. *J Biomed Mater Res B Appl Biomater.* 2009;91(2):938–47.
40. Petersen LK, Ramer-Tait AE, Broderick SR, Kong CS, Ulery BD, Rajan K, *et al.* Activation of innate immune responses in a pathogen-mimicking manner by amphiphilic polyanhydride nanoparticle adjuvants. *Biomaterials.* 2011;32(28):6815–22.
41. O'Bryan T, Weiher H, Rennke HG, Kren S, Hostetter TH. Course of renal injury in the Mpv17-deficient transgenic mouse. *J Am Soc Nephrol.* 2000;11(6):1067–74.
42. Dunn SR, Qi Z, Bottinger EP, Breyer MD, Sharma K. Utility of endogenous creatinine clearance as a measure of renal function in mice. *Kidney Int.* 2004;65(5):1959–67.
43. Eaton KA, Friedman DI, Francis GJ, Tyler JS, Young VB, Haeger J, *et al.* Pathogenesis of renal disease due to enterohemorrhagic *Escherichia coli* in germ-free mice. *Infect Immun.* 2008;76(7):3054–63.
44. Lee PY, Wang JX, Parisini E, Dascher CC, Nigrovic PA. Ly6 family proteins in neutrophil biology. *J Leukoc Biol.* 2013;94(4):585–94.
45. Lai L, Alaverdi N, Maltais L, Morse 3rd HC. Mouse cell surface antigens: nomenclature and immunophenotyping. *J Immunol.* 1998;160(8):3861–8.
46. Vermaelen K, Pauwels R. Pulmonary dendritic cells. *Am J Respir Crit Care Med.* 2005;172(5):530–51.
47. Lohmann-Matthes ML, Steinmuller C, Franke-Ullmann G. Pulmonary macrophages. *Eur Respir J.* 1994;7(9):1678–89.
48. Petersen LK, Phanse Y, Ramer-Tait AE, Wannemuehler MJ, Narasimhan B. Amphiphilic polyanhydride nanoparticles stabilize *Bacillus anthracis* protective antigen. *Mol Pharm.* 2012;9(4):874–82.
49. Haughney SL, Petersen LK, Schoofs AD, Ramer-Tait AE, King JD, Briles DE, *et al.* Retention of structure, antigenicity, and biological function of pneumococcal surface protein A (PspA) released from polyanhydride nanoparticles. *Acta Biomater.* 2013;9(9):8262–71.
50. Harush-Frenkel O, Bivas-Benita M, Nassar T, Springer C, Sherman Y, Avital A, *et al.* A safety and tolerability study of differently-charged nanoparticles for local pulmonary drug delivery. *Toxicol Appl Pharmacol.* 2010;246(1–2):83–90.
51. Nguyen J, Reul R, Betz T, Dayyoub E, Schmehl T, Gessler T, *et al.* Nanocomposites of lung surfactant and biodegradable cationic nanoparticles improve transfection efficiency to lung cells. *J Control Release.* 2009;140(1):47–54.
52. Alarifi S, Ali D, Al-Doaiss AA, Ali BA, Ahmed M, Al-Khedhairy AA. Histologic and apoptotic changes induced by titanium dioxide nanoparticles in the livers of rats. *Int J Nanomedicine.* 2013;8:3937–43.
53. Yamagishi Y, Watari A, Hayata Y, Li X, Kondoh M, Yoshioka Y, *et al.* Acute and chronic nephrotoxicity of platinum nanoparticles in mice. *Nanoscale Res Lett.* 2013;8(1):395.
54. Kelley VE, Winkelstein A. Age- and sex-related glomerulonephritis in New Zealand white mice. *Clin Immunol Immunopathol.* 1980;16(2):142–50.
55. Yang Y, Pan D, Luo K, Li L, Gu Z. Biodegradable and amphiphilic block copolymer-doxorubicin conjugate as polymeric nanoscale drug delivery vehicle for breast cancer therapy. *Biomaterials.* 2013;34(33):8430–43.
56. Italia JL, Bhatt DK, Bhardwaj V, Tikoo K, Kumar MN. PLGA nanoparticles for oral delivery of cyclosporine: nephrotoxicity and pharmacokinetic studies in comparison to Sandimmune Neoral. *J Control Release.* 2007;119(2):197–206.
57. Zhang XD, Wu D, Shen X, Liu PX, Fan FY, Fan SJ. In vivo renal clearance, biodistribution, toxicity of gold nanoclusters. *Biomaterials.* 2012;33(18):4628–38.
58. Goldstein SL. Urinary kidney injury biomarkers and urine creatinine normalization: a false premise or not? *Kidney Int.* 2010;78(5):433–5.
59. Peralta CA, Shlipak MG, Judd S, Cushman M, McClellan W, Zakai NA, *et al.* Detection of chronic kidney disease with creatinine, cystatin C, and urine albumin-to-creatinine ratio and association with progression to end-stage renal disease and mortality. *JAMA.* 2011;305(15):1545–52.
60. Waikar SS, Sabbiseti VS, Bonventre JV. Normalization of urinary biomarkers to creatinine during changes in glomerular filtration rate. *Kidney Int.* 2010;78(5):486–94.
61. Nemmar A, Hoylaerts MF, Hoet PH, Vermeylen J, Nemery B. Size effect of intratracheally instilled particles on pulmonary inflammation and vascular thrombosis. *Toxicol Appl Pharmacol.* 2003;186(1):38–45.
62. Heyder J, Gebhart J, Rudolf G, Schiller CF, Stahlhofen W. Deposition of particles in the human respiratory tract in the size range 0.005–15 μm . *J Aerosol Sci.* 1986;17(5):811–25.
63. Hofmann W. Modelling inhaled particle deposition in the human lung—a review. *J Aerosol Sci.* 2011;42(10):693–724.
64. Choi HS, Ashitate Y, Lee JH, Kim SH, Matsui A, Insin N, *et al.* Rapid translocation of nanoparticles from the lung airspaces to the body. *Nat Biotechnol.* 2010;28(12):1300–3.
65. Ulery BD, Petersen LK, Phanse Y, Kong CS, Broderick SR, Kumar D, *et al.* Rational design of pathogen-mimicking amphiphilic materials as nanoadjuvants. *Sci Rep.* 2011;1:198.
66. Dailey LA, Jekel N, Fink L, Gessler T, Schmehl T, Wittmar M, *et al.* Investigation of the proinflammatory potential of biodegradable nanoparticle drug delivery systems in the lung. *Toxicol Appl Pharmacol.* 2006;215(1):100–8.

67. Xing Z, Gauldie J, Cox G, Baumann H, Jordana M, Lei XF, *et al.* IL-6 is an antiinflammatory cytokine required for controlling local or systemic acute inflammatory responses. *J Clin Invest.* 1998;101(2):311–20.
68. Coelho AL, Hogaboam CM, Kunkel SL. Chemokines provide the sustained inflammatory bridge between innate and acquired immunity. *Cytokine Growth Factor Rev.* 2005;16(6):553–60.
69. Frevert CW, Huang S, Danaee H, Paulauskis JD, Kobzik L. Functional characterization of the rat chemokine KC and its importance in neutrophil recruitment in a rat model of pulmonary inflammation. *J Immunol.* 1995;154(1):335–44.